



HAL
open science

Nanofabrication of Au nanoparticles over conductive metallohydrogel nanofibers for nanocatalysis application

Manish Kumar Dixit, Déborah Chery, Chinthakuntla Mahendar, Christophe Bucher, Mrigendra Dubey

► **To cite this version:**

Manish Kumar Dixit, Déborah Chery, Chinthakuntla Mahendar, Christophe Bucher, Mrigendra Dubey. Nanofabrication of Au nanoparticles over conductive metallohydrogel nanofibers for nanocatalysis application. *Inorganic Chemistry Frontiers*, 2020, 7 (4), pp.991-1002. 10.1039/C9QI01514K . hal-03033283

HAL Id: hal-03033283

<https://hal.science/hal-03033283>

Submitted on 4 Jan 2021

HAL is a multi-disciplinary open access archive for the deposit and dissemination of scientific research documents, whether they are published or not. The documents may come from teaching and research institutions in France or abroad, or from public or private research centers.

L'archive ouverte pluridisciplinaire **HAL**, est destinée au dépôt et à la diffusion de documents scientifiques de niveau recherche, publiés ou non, émanant des établissements d'enseignement et de recherche français ou étrangers, des laboratoires publics ou privés.

Multi-stimuli responsive conductive coordination polymeric metallohydrogel: Nanofabrication and catalysis

Manish Kumar Dixit, Déborah Chery, Christophe Bucher and Mrigendra Dubey*

Abstract: A multi stimuli-responsive conductive and fluorescent metallohydrogel involving coordination polymers (1% w/v, CPH) has been synthesized from non-fluorescent components *viz.*, an L-tyrosine derived ligand (**1**), LiOH and Zn(NO₃)₂ used in 1:3:1 proportions at pH 11-12. CPH shows reversible gel-sol transitions in response to external stimuli including thermal, mechanical and ultrasound stress. CPH also exhibit good shape persistence and reswelling properties. The formation of true gel phase was established on the ground of detailed rheological experiments. Each steps involved in the formation of CPH, including initial coordination, polymerization, aggregation, nanofiber growth followed by gelation, have been thoroughly explored by FTIR, fluorescence, TEM, PXRD, NMR, TGA and Mass spectrometry measurements. The availability of –COOH and –NH functional groups onto the nanofibers surface has been shown to provide favourable chemical environments for the formation of ultra-thin and uniform sized (~3 nm) gold nanoparticles (AuNPs). AuNPs embedded in CPH gel matrix (AuCPH) were also found useful as catalysts in the reduction of *p*-nitrophenol by mild reducing agents like NaBH₄. This effect was brought to light with an estimation of the rate constant and activation energy of the reduction reaction estimated at 0.223 min⁻¹/58.94 KJmol⁻¹ in the presence of AuCPH and at 0.014 min⁻¹/595.14 KJmol⁻¹, in the absence of AuCPH. Conductivity values reaching 5.05x10⁻³ S cm⁻¹ and 4.18x10⁻³ S cm⁻¹ at 295 K have been determined for AuNp-doped and AuNp-free metallohydrogels, respectively.

Introduction

Metallogels have emerged in the last few years as an important and exciting new class of soft materials. Their construction usually involve coordination bonds as growth driver, eventually supplemented by additional non-covalent interactions such as H-bonds, Van der Waals interactions or host-guest recognition processes.¹ Many previous studies have established that the

dynamic and reversible features of most metal-ligand bonds are key to the development of stimuli-responsive metallogels for applications in drug delivery, pollutant removal and sensing.^{1e-1h} Inclusion of metal ions into organic gels also proved beneficial in providing additional morphological, spectroscopic, rheological, electrical,^{2e,4} magnetic or catalytic properties or for application in gas/dye adsorption, crystal growth and guest encapsulation.² A few metallogels have also been used as media for carrying out investigations on Au and Ag nanoparticles.^{2f-2h}

As a general statement, conductive soft materials are of utmost importance for energy conversion and storage purposes. They find useful applications in batteries, fuel cells, electrochemical supercapacitors, solar cell and electronic skin.³ In that regard, the conductance as an inherent property of metallogels has recently become a subject of increasing attention.^{2e,4} The most conductive gels⁵ reported so far exhibit conductivity values ranging from 10⁻⁴ to 10⁻² S cm⁻¹. Moreover, the high conductivity measured in the gel states usually involve conventional polymers^{5b}/molecules^{5d,e} or doping with suitable additives^{5f}. Some gels have also been shown to behave as protons conductors, with conductivity values falling in the range of 2.4x10⁻² to 1.4 x10⁻⁴ S cm⁻¹ in the xerogel state. In line with these issues, we have recently reported the ultrasound-induced formation of metallogels coming along with an unprecedented ~10 fold enhancement in the conductivity values going from 0.45 to 4.06 x10⁻⁴ S cm⁻¹.^{2e} However, the design and synthesis of highly conductive metallogels still remains a challenging task.⁶

Over the last decade, metallogels have also proved useful as active material in catalytic reactions.⁷ There have indeed been an increased focus on hybrid metallogels containing catalytically-active NPs. Steed, Jung *et al.* have disjointedly reported some early examples of such achievements, with the *in situ* growth of Ag nanoparticles in metallogel matrix used as nanocatalyst in reduction reactions.^{2f-2g} Also, a series of Tris(pyridylamide)-based metallogels have recently been used as a media for studying the growth and the catalytic properties of silver nanoparticles in the reduction of *p*-nitrophenolate to *p*-aminophenolate. The size/surface area of nanoparticles is a key parameter in nanocatalysis and a number of previous reports have revealed that the fibres present in metallogels can be used as templates to control the growth of Nps.^{2f-2h} Further, the growth and selective deposition of nanoparticles over gel fibers directed by functional groups introduced on gelators has been recently reported.^{2f-2h} (Cb : I would delete this last sentence. As it says the Same as the one before)In most cases, the apparent rate constants (K_{app}) reported for reduction reactions involving Au nanoparticles as catalyst ranges from 0.05 to ~2.5 min⁻¹.⁸ The handful of articles mentioned above show that the controlled growth of Au Nps in

Dr. Mrigendra Dubey
Soft Materials Research Laboratory, Discipline of Metallurgy Engineering and Materials Science, Indian Institute of Technology Indore, Khandwa Road, Simrol, Indore 453552, India
E-mail: mdubey@iiti.ac.in

Dr. Christophe Bucher and Dr. Deborah Chery
Univ Lyon, Ens de Lyon, CNRS UMR 5182, Université Claude Bernard Lyon 1, Laboratoire de Chimie, Lyon, France

Mr. Manish Kumar Dixit
Department of Chemistry, Indian Institute of Technology (Banaras Hindu University), Varanasi 221005, U.P., India

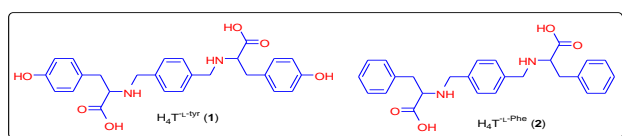
Supporting information for this article is given via a link at the end of the document. ((Please delete this text if not appropriate))

FULL PAPER

metallogel-based matrices for application in catalysis is a challenging task.

Besides, none of the studies reported so far involve coordination polymers metallohydrogels displaying simultaneously stimuli responsiveness, fluorescent, catalytic and conductance properties.

In line with the above mentioned issues and challenges, we report here on the synthesis and properties of stimuli-responsive fluorescent coordination polymer metallohydrogels (**CPH**) obtained from sequential mixing of LiOH and Zn(NO₃)₂ to a L-tyrosine derived low molecular weight gelator H₄T^{L-tyr} (**1**) (scheme 1). This study also includes the nanofabrication of Au nanoparticles used as active sites in the catalytic reduction of *p*-nitrophenol and conductance measurements carried out on gels samples.



Scheme 1: Structures of the title compounds **1** (H₄T^{L-tyr}) and **2** (H₄T^{L-Phe}).

Results and Discussion

The chiral low molecular weight ligands H₄T^{L-tyr} (**1**) and H₄T^{L-Phe} (**2**) have been obtained in good yields from L-Tyrosine and L-Phenylalanine amino acids, respectively (See Scheme S1 in supporting information). We found that transparent metallohydrogels (**CPH**, 1% w/v) readily form at pH 11–12 and ambient temperature after deprotonation of **1** with an aqueous solution of LiOH·H₂O followed by gradual addition of Zn(NO₃)₂·6H₂O in a 1:3:1 ratio (see the experimental section for details). The gel was preliminary tested by standard methods like the ‘inverted vial’ and ‘falling ball’ tests (Figure 1). The key role of alkali ions in the gelation process was revealed upon substituting Li⁺ for Na⁺, K⁺ or Cs⁺ and finding out that such replacements result in a significant increase of the gelation time and in a decrease of the gel strength, which might be due to the high hydration capability of Li⁺ compared to the other alkali metal ions.^{2e,9} It is also further supported by the fact that non-alkali bases like, TBAOH, NH₃ or Et₃N failed to produce gels (See Figure S1 and S2 in supporting information).

Formation of **CPH** was also found to require the presence of water as a solvent and of Zn(NO₃)₂ as an assembling element. The importance of both the cation and the anion species was brought to light with all our attempts to replace either Zn²⁺ or NO₃⁻ ions failing to produce gels (Table S1, Supporting Information). Then, use of ligand **2** (H₄T^{L-Phe} in scheme 1) instead of **1** only led to the formation of gelatinous solutions, which suggests the implication of the –OH groups in the gelation process (See Figure S1 in supporting information). The synthesis of **CPH** was thus found to exhibit a multi-dimensional selectivity *viz.* towards ligand, base, Zn(NO₃)₂, solvent and pH. The freshly synthesized **CPH** was transparent enough to read a text through it and was found to emit blue light when exposed to UV irradiations of λ = 365 nm (See Figure S3 in supporting information). Gel-sol phase

transitions **could also be** reversibly triggered using external stimuli such as temperature, ultrasound and mechanical force (See Figure S3 in supporting information). Another material benefit of the **CPH gels** is that it can be stored at 20 °C for more than a year without change in appearance or transparency.

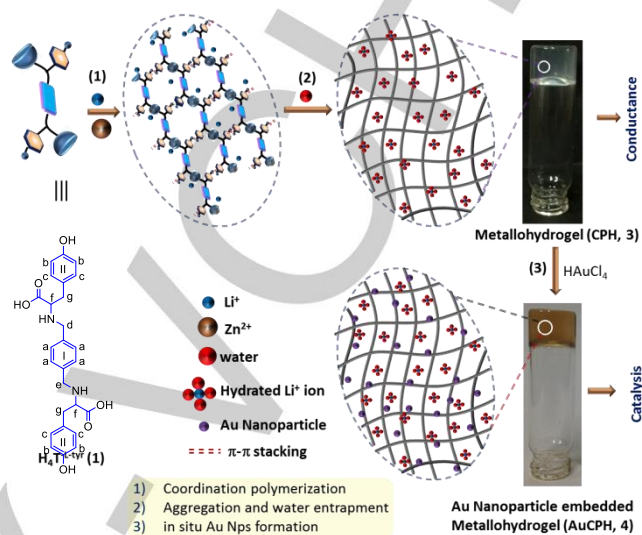


Figure 1. Pictorial presentation of mechanism involved in gelation and properties obtained in metallohydrogel.

We also discovered that dark pink gold nanoparticles (NPs) can be grown inside **CPH** matrix in the absence of reducing agent, by simple addition of a methanolic/ether solution of HAuCl₄ (Figure 1). Formation of AuNps was unambiguously demonstrated by the observation of a diagnostic surface plasmon resonance (SPR) signal centered at ca. 560 nm (See Figure S4 in supporting information).¹⁰ As for the formation mechanism, the reduction of Au(III) to Au(0) and the subsequent deposition of the nanoparticles over the supramolecular nanofibers, although not fully understood, might potentially be achieved through the oxidation of the electron donating amine functions available in **1**.^{2f,11} A detailed characterization of the **CPH** and **AuCPH** materials is provided in the following sections. It also includes catalytic studies, where freshly prepared AuNp-doped CPH proved useful to achieve the reduction of *p*-nitrophenol into the corresponding aminophenol (Figure 7).

Morphological characterization

Transmission electron microscopy (TEM) measurements provided key insights into the morphology of **CPH** (**3**) and **AuCPH** (**4**) (Figure 2, Figure S5 and S6 in supporting information). Images recorded with **CPH** (**3**) revealed a uniform and long-range branched nano-fibrous morphology, with an average fiber diameter of ~20 nm. In **AuCPH** (**4**), the observation of nanometer-size AuNPs (~3nm), with an apparent narrow size distribution, uniformly deposited over the fibers suggests the key role of the chemical functions available at the surface of the fibers in directing the reduction-induced growth of the NPs. Dynamic Light

FULL PAPER

Scattering (DLS) analyses conducted on AuCPH (**4**) unfortunately failed to provide the exact size distribution of the AuNps, most probably due to presence of nanofibers inside the gel matrix.

X-ray powder diffraction (PXRD) experiments have been carried out with the metal free ligand **1** and with dried CPH samples to gain further insights into the arrangement and packing pattern of the nanofibers. The PXRD pattern collected with $\text{H}_4\text{T}^{-\text{yr}}$, displays intense crystalline peaks at $2\theta = 8^\circ, 17^\circ, 20^\circ, 21.5^\circ, 26^\circ$ (See Figure S17 in supporting information). The pattern recorded with xerogels obtained from CPH includes a broad diffraction peak centered at 20° accounting for the amorphous nature of the dried gel¹² and an intense peak at 21.22° consistent with the presence of stacking pattern in CPH with a d -spacing value of 4.18 \AA .¹³ Then, the reflection observed at 3.82 \AA ($2\theta = 23.24^\circ$) is attributed to a regular stacking (π - π) of the individual ligands in the fibers.¹⁴ The pattern also includes a series of peaks (d -spacing ranging from 2.3 - 2.83 \AA) assigned to hydrogen bonding interactions involved in the formation of fibers and in the gelification.^{14b}

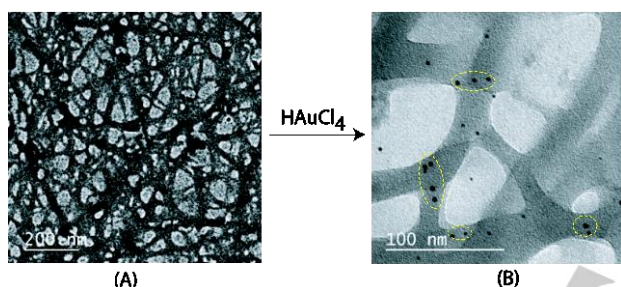


Figure 2. TEM images of metallogel CPH (A) and of AuCPH (B) revealing the presence of AuNPs located onto the fibers.

Aggregation studies

Fluorescence measurements have been carried out to further characterize the chemical processes involved in the formation of CPH. The fluorescence spectra of LiOH deprotonated **1** ($1 \times 10^{-2} \text{ M}$, H_2O , $\lambda_{\text{ex}} = 275 \text{ nm}$) showed two peaks centered at 330 nm (Stokes shift = 6000 cm^{-1}) and 408 nm (Stokes shift = 11800 cm^{-1}) attributed to π - π^* and n - π^* transitions, respectively. Addition of increasing amounts of $\text{Zn}(\text{NO}_3)_2$ (1 M solution in H_2O) led to a blue shift of about 7 nm of both emission signals coming along with a significant enhancement ($\sim +90\%$) in intensity (Figure 3). The latter effect is attributed to a reduction of the non-radiative decay through a rigidification of the ligand backbone upon chelation with Zn^{2+} .¹⁵ The fact that the emission intensity at 330 nm , associated to π - π^* transitions, increases to a much larger extent than that recorded at 408 nm also suggest that π - π stacking interactions are involved in the aggregation process leading to gelation (Figure 3).

Similar investigations carried out on non-gelling combinations of ligand/base/metal, viz: $1/\text{Cs}^+/\text{Zn}^{2+}$, $1/\text{TBAOH}/\text{Zn}^{2+}$, $1/\text{Li}^+/\text{Zn}(\text{OAc})_2$ and $1/\text{Li}^+/\text{Cu}^{2+}$, served to confirm the selectivity of the gelation process towards each components (See Figure S8 and Figure S9 in supporting

information). The importance of lithium ions in the gelification of $1/\text{Li}^+/\text{Zn}(\text{NO}_3)_2$ mixtures was revealed upon showing that the substitution of Li^+ with any other alkali ion yielded clear ungelified solutions coming along with a decrease in the intensity of both emission signals (See Figure 3 and S8 in supporting information). Then, addition of Zn^{2+} to ligand **2** in the same conditions as above was found to result in a much lower increase ($\sim +40\%$) of the emission signals centered at 328 nm (Stokes shift = 8300 cm^{-1}) and 396 nm (Stokes shift = 13500 cm^{-1}). Formation of zinc adducts with **2** also led to a red shift of about 11 nm of the emission band at higher energy (π - π^*), to be compared to the 7 nm blue shift observed in the same conditions with **1**, which is in agreement with the formation of two distinct molecular arrangement (See Figure S10 and S13 in supporting information).

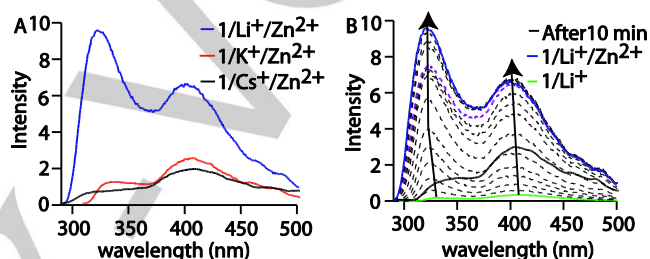


Figure 3. (A) A fluorescence spectra of **1** with $\text{Li}^+/\text{Zn}^{2+}$ (blue line), $\text{K}^+/\text{Zn}^{2+}$ (red line) and $\text{Cs}^+/\text{Zn}^{2+}$ (black line) in water, (B) Titration between $1/\text{Li}^+$ vs Zn^{2+} (1 , ($\lambda_{\text{ex}} = 275 \text{ nm}$, $1 \times 10^{-2} \text{ M}$, H_2O ; LiOH , $3 \times 10^{-2} \text{ M}$, H_2O ; $\text{Zn}(\text{NO}_3)_2$, $1 \times 10^{-2} \text{ M}$, H_2O).

The aggregation process involved in the formation of CPH was further demonstrated upon carrying out fluorescence measurements ($\lambda_{\text{ex}} = 275 \text{ nm}$) on gel samples obtained at different concentrations. The curves collected in figure 4 have been recorded after multiple dilutions of a freshly prepared CPH gel, from 10^{-2} M (red line) down to $5 \times 10^{-4} \text{ M}$ (black line). These data reveal that dilution results in a large increase in the emission intensity at 338 nm (π - π^*) associated to a continuous blue shift of the maximum emission wavelength (reaching 22 nm at $0.5 \times 10^{-3} \text{ M}$), the latter changes being observed while the emission peak at 411 nm (n - π^*) remained unchanged throughout the dilution experiment. The emission at 338 nm was found to reach a maximum value at about $0.5 \times 10^{-3} \text{ M}$ and then to go down with further dilution to lose about 90% of its initial intensity at $1 \times 10^{-4} \text{ M}$. This drastic drop in intensity is here also associated to a continuous blue shift of the max wavelength going from 311 to 307 nm when concentration is decreased from $0.5 \times 10^{-3} \text{ M}$ to $1 \times 10^{-4} \text{ M}$. The successive increase and decrease of the emission intensity observed upon dilution of the gel can be attributed to a combination of segregation and dilution effects. The increase in intensity observed with increasing dilution, i.e. from 1×10^{-2} to $0.5 \times 10^{-3} \text{ M}$, is attributed to a minimization of the aggregation caused quenching (ACQ) phenomena promoted by the gelification process.¹⁶ Then the intensity drop observed at the lower end

of the concentration range (0.5×10^{-3} to 1×10^{-4} M) is attributed to a simple dilution of the fluorescent entities.

The overall blue shift of about 31 nm observed over the entire dilution range is most probably related to changes in the π - π stacking modes ultimately leading to aggregation followed by gelification, an assumption which is consistent with the results obtained from PXRD experiments.

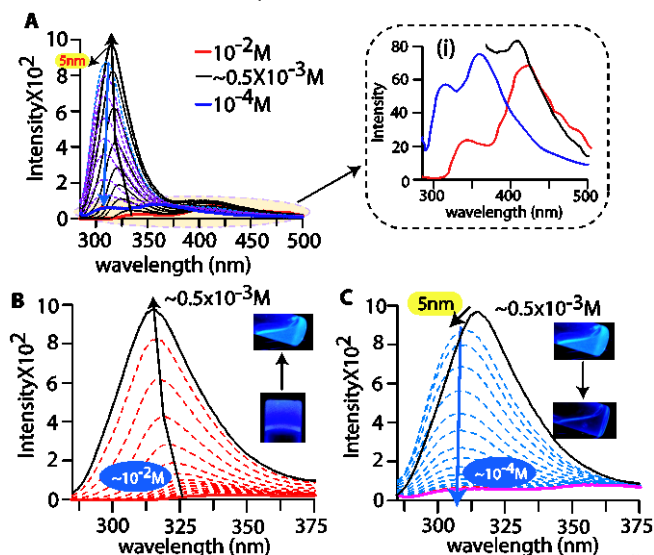


Figure 4. Dilution experiments followed by fluorescence spectroscopy (A) dilution of CPH from 10^{-2} (red line) to 10^{-4} (blue line) M, (i) is inset of A. (B) dilution up to $\sim 0.5 \times 10^{-3}$ M (black line) along with pictures of the gel and diluted gel under UV light and (C) further dilution down to 10^{-4} M (blue line) and pictures of the corresponding vial under UV light.

The interactions involved in the aggregation and gelation process have been further investigated by ^1H NMR spectroscopy. The titration of **1** (1.4×10^{-2} M, $400 \mu\text{L}$, deprotonated with 1.5 molar equivalents of LiOH) with Zn^{2+} (2.8×10^{-2} M, $200 \mu\text{L}$) has been carried in D_2O (See Figure S13 in supporting information). It needs to be mentioned that the deprotonation of **1** with LiOH is required to enhance the solubility of the ligand in D_2O and to enable the formation of Zn^{2+} complexes. As expected, the spectrum of the deprotonated ligand **1** shows seven signals resonating at $\delta_a = 7.27$ ppm (d, 4H, -Ph₁), $\delta_b = 6.95$ ppm (d, 4H, -PhOH), $\delta_c = 6.54$ ppm (d, 4H, -Ph), $\delta_d = 3.72$ ppm (d, 2H, -CH₂Ph), $\delta_e = 3.54$ ppm (d, 2H, -CH₂Ph), $\delta_f = 3.28$ ppm (t, 2H, -CHNH) and $\delta_g = 2.75$ ppm (m, 4H, -CH₂NH) ppm. Adding aliquots of a stock solution of Zn^{2+} to the aforementioned sample was found to induce a significant broadening of all the signals accompanied by downfield shifts reaching maximum values ($\Delta\delta_c = 0.15$ ppm $>$ $\Delta\delta_b = 0.07$ ppm $>$ $\Delta\delta_g \sim \Delta\delta_d = 0.05$ ppm) after addition of 1 molar equivalent of metal, which is in agreement with the formation of 1:1 (**1**: Zn^{2+}) coordination complexes. The largest downfield shift observed for the phenolic ring protons (H_c and H_b) is attributed to π - π interactions between phenolic rings presumably arranged in antiparallel stacks, a conclusion which is also supported by

the PXRD and fluorescence data discussed above (See figure S13 in Supporting Information). By analogy, the small downfield shift $\Delta\delta_a = 0.0306$ ppm observed for the protons of the central benzene ('l' in Figure 1) suggests a limited interaction of this aromatic ring with its closest neighbours¹⁷ At the same time, the downfield shift observed for the signals attributed to the aliphatic protons and to the 'l' benzene ring protons is due to a decrease of the electron density in ligand **1** induced by its coordination to the Zn^{2+} ions.¹⁸ The broadening of all the signals and the concomitant decrease of the signal-to-noise (S/N) ratio observed in the presence of Zn^{2+} is attributed to a significant increase in the viscosity on account of the gelation process.¹⁹

Complexation analysis

A comparative FT-IR spectroscopic analysis of **1** and of the related xerogel was conducted to assess the role of each functional group in the gelation process. The FT IR spectrum of **1** displays intense vibration peaks centered at $\nu_{\text{as}}(\text{COO}) = 1615$ cm^{-1} , $\nu_b(-\text{CH}) = 1455$ cm^{-1} , $\nu_b(-\text{OH}, \text{phenolic}) = 1331$ cm^{-1} and $\nu_{\text{str}}(\text{C-N}) = 1258$ cm^{-1} . In the xerogel, these characteristic peaks appear shifted at $\nu_{\text{as}}(\text{COO}) = 1631$ cm^{-1} ($\Delta\nu = 16$ cm^{-1}), $\nu(-\text{CH}) = 1441$ cm^{-1} ($\Delta\nu = 14$ cm^{-1}), $\nu_b(-\text{OH}, \text{phenolic})$ absent and $\nu_{\text{str}}(\text{C-N}) = 1247$ cm^{-1} ($\Delta\nu = 11$ cm^{-1}). Other key features include the absence of the bending vibration mode of the phenolic -OH, consistent with its deprotonation with LiOH, and the observation of a broad peak at ~ 3400 attributed to water molecules trapped within the gel matrix (Figure S14 in supporting information). The significant shift of most vibrations supports the existence of interactions between the $>\text{C}=\text{O}$, -NH and -OH moieties with the Li^+ and Zn^{2+} cations all along the gelation process.

Similar studies have been conducted with xerogels obtained from **CPH** and from **AuCPH**, mainly to gain insights into the interactions involved between $[\text{1}/\text{Zn}^{2+}]$ and the AuNps (See Figure S15 in supporting information). The main difference observed between the FTIR spectra of both samples is the large shift of the diagnostic $\nu_{\text{as}}(\text{COO})$ vibration, from 1631 cm^{-1} to 1615 cm^{-1} , associated to the formation of AuNPs. This clear experimental evidence support the conclusion that the carbonyl units are available over the surface of the nanofibers in the **CPH** gel and that they are involved in the directed growth of AuNPs (figure 6).

The formation of coordination polymers and the stoichiometry of the association between **1** and Zn^{2+} have been scrutinized by absorption spectroscopy and by ESI-MS measurements. The method of continuous variation, also known as the Job's method, has been used to estimate the stoichiometry of the association.²⁰ Plotting the absorbance at 402 nm, which correlates with the concentration of complex formed in solution, as a function of the molar ratio $x = [\text{Zn}^{II}]/([\text{Zn}^{II}] + [\text{T}^{-\text{by}}])$ calculated at constant volume, led to the triangle shaped curve depicted in figure 5B. The angular curvature of this plot featuring a max value at $x = 0.5$ is fully consistent with a strong binding between **1** and Zn^{2+} in a 1:1

ratio (Figure 5). This stoichiometry was further confirmed by analysis of the ESI-MS spectrum of **CPH**, showing a peak at $m/z = 527.1$ attributed to the 1:1 coordination complex $[\text{H}_3\text{T}^{\text{L-tyr}} + \text{Zn}]^+$ (calcd. $m/z = 527.1$), observed here as the repeating unit of the coordination polymer involved in metallohydrogel (Figure 5). The metal-driven self-assembly and the polymeric nature of the metallohydrogel is furthermore revealed through the observation of additional peaks at regular m/z intervals like at $m/z = 615.1$ ($[(\text{H}_3\text{T}^{\text{L-tyr}}/\text{Li} + \text{Zn}/\text{NO}_3/\text{H}_2\text{O})]^+$, calcd. $m/z = 615.1$), $m/z = 675.0$ ($[(\text{H}_2\text{T}^{\text{L-tyr}}/\text{Zn}_2 + \text{NO}_3/\text{H}_2\text{O})]^+$, calcd. $m/z = 675.2$), $m/z = 991.3$ ($[(\text{H}_3\text{T}^{\text{L-tyr}})_2/\text{Zn}/\text{H}]^+$, calcd. $m/z = 991.3$), $m/z = 1063.2$ ($[(\text{H}_2\text{T}^{\text{L-tyr}})_2/\text{Li}/\text{Zn}_2]^+$, calcd. $m/z = 1063.2$) and $m/z = 1119.1$ ($[(\text{H}_2\text{T}^{\text{L-tyr}})_2/\text{Zn}_3/\text{H}]^+$, calcd. $m/z = 1119.3$) (See figure S16 in supporting information). Taken together, the MS and Job's plot analyses support the conclusion that a 1:1 complexation between **1** and Zn^{2+} leads to the formation of long range coordination polymers self-arranged into fiber-shaped nanostructures involved in the gelation.

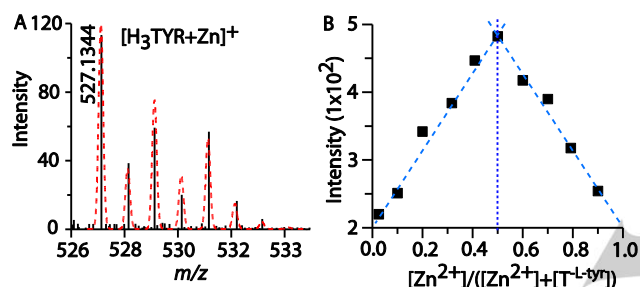


Figure 5. (A) ESI-MS spectra of asymmetric unit represents the experimental isotopic abundance pattern (black line) and simulated (red dotted line) and (B) Job's plot for LiOH deprotonated **1** vs. $\text{Zn}(\text{NO}_3)_2$.

Nanofabrication and catalysis

Metal-organic gel CPH samples have been used to achieve the synthesis of hybrid AuNPs-modified Nanofibers. The addition of a freshly prepared solution of HAuCl_4 (methanol/ether mixture) to the CPH gel sample kept under stirring led to an instantaneous color change from colorless to red brown, consistent with the formation of AuNPs inside the gel matrix (See figure S17 in supporting information). The latter AuNPs were submitted to in-depth characterizations using SPR (ca. 560 nm) and TEM (*vide infra*). The latter studies revealed that using CPH gel as a medium enables a size-selective (~3 nm) and homogeneous growth of AuNPs throughout the sample, most probably due to the presence of suitable growth-directing functional groups uniformly distributed at the surface of the nanofibers. The size distribution is one of the most important parameter for applications in nanoparticle-based catalysis.^{7e} The catalytic activity of the gel-embedded AuNPs has been evaluated towards the reduction of *p*-nitrophenol in the presence of NaBH_4 . The progress and kinetics of the reaction have been followed/calculated from UV-Vis absorption data recorded throughout the reaction. Addition of increasing

amounts of NaBH_4 (15 mM in water) to *p*-nitrophenol (0.15mM in water H_2O) in the absence of AuNPs led to a significant modification of the absorption spectrum of the solution (going from light to intense yellow), including a loss of the initial signal at 318 nm at the expense of a new signal growing at 400 nm attributed to the accumulation of *p*-nitrophenolate ion (Figure 7).²¹ Further addition of NaBH_4 , up to 10 molar equivalents, proved ineffective in promoting additional changes in the spectroscopic signature of the sample, even after 1 hour at room temperature, which confirms that a catalyst is needed to achieve the reduction of *p*-nitrophenol into *p*-aminophenol.

The same experiment carried out in the presence of catalytic amount of freshly prepared AuCPH (20 μL added to 2 mL reaction mixture) led to a fast decrease in the absorbance at $\lambda_{\text{max}} = 400$ nm coming along with clean isosbestic points at 281 and 312 nm. It also led to the emergence of new peaks centered at 278 and 283 nm attributed to the conversion of *p*-nitrophenolate leading to the accumulation of *p*-aminophenol.²¹ In our experimental conditions (2 mL of *p*-nitrophenol, 10 molar equ. of NaBH_4 , room temperature) a complete conversion was achieved in less than 7 minutes in the presence of a catalytic amount of AuCPH. In agreement with a pseudo first-order rate law, the kinetics of the reduction reaction was estimated from the linear plot of $\ln(A_t/A_0)$ vs time, where A_0 and A_t stand for the initial absorbance at $t=0$ and for the absorbance at $t > 0$, respectively (Figure 7).²¹ The apparent rate constant k_{app} corresponding to this pseudo first-order kinetics could be estimated at 305 K to 0.223 min^{-1} using equation 1. From the data shown in figure 7 and 8 and equation 2 and 3, the E_a , ΔS^\ddagger and ΔH^\ddagger values corresponding to the AuCPH-catalyzed reduction of *p*-nitrophenol have then been estimated at 58.94 KJmol^{-1} , $244.09 \text{ Jmol}^{-1}\text{K}^{-1}$ and 4.41 KJ mol^{-1} , respectively. These data fall in the range of energies reported in previous studies on nanoparticle-based reduction reactions.^{7,22} The k_{app} , E_a , ΔS^\ddagger and ΔH^\ddagger values estimated for the same NaBH_4 mediated reduction reaction studied in the absence of AuCPH were found to be 0.014 min^{-1} , $595.14 \text{ KJmol}^{-1}$, $-261.96 \text{ Jmol}^{-1}\text{K}^{-1}$ and 5.66 JK^{-1} , respectively. Thus, comparative kinetics data collected with and without using AuCPH clearly demonstrate the beneficial role of AuCPH as catalyst in the reduction of *p*-nitrophenol reaction.

$$\ln\left(\frac{A_t}{A_0}\right) = -k_{\text{app}}t \quad (\text{Equ. 1})$$

$$\ln k_{\text{app}} = \ln A - \frac{E_a}{RT} \quad (\text{Equ. 2})$$

$$\ln\left(\frac{k_{\text{app}}}{T}\right) = \ln\left(\frac{k_B}{T}\right) + \frac{\Delta S^\ddagger}{T} - \frac{\Delta H^\ddagger}{T} \left(\frac{1}{T}\right) \quad (\text{Equ. 3})$$

Where E_a stands for the activation energy, A for the Arrhenius constant, R for the gas constant, T for temperature, ΔS^\ddagger for the activation entropy and ΔH^\ddagger for the activation enthalpy.²²

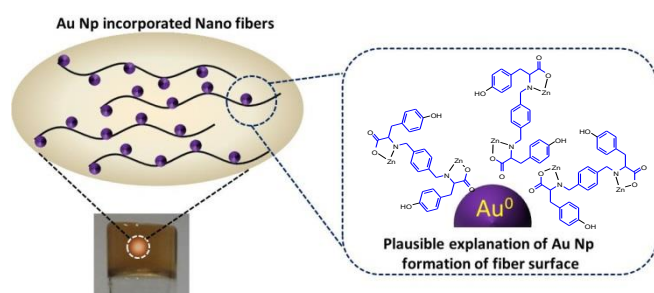


Figure 6. Schematic presentation of Au nanoparticle formation over nanofiber.

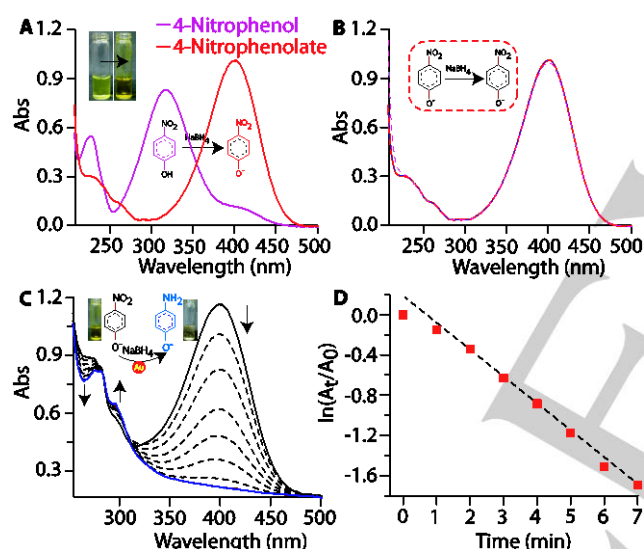


Figure 7. (A) *p*-nitrophenol (0.15 mM) before (violet line) and after (red line) addition of NaBH₄ (15 mM) solution; (B) 0.15 mM *p*-nitrophenolate with NaBH₄ (15 mM) without AuNp as catalyst, (C) Reduction of *p*-nitrophenolate (0.15 mM) with NaBH₄ (15 mM) in the presence of AuNPs as catalyst originated from AuCPH at room temperature, (D) Plot of $\ln(A_t/A_0)$ vs. reaction time (min) showing pseudo-first order kinetics for metallogel.

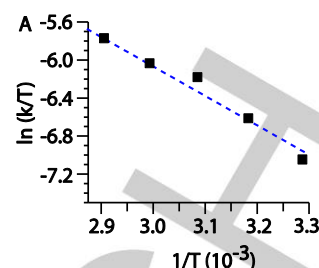


Figure 8. Arrhenius plot for reduction of *p*-nitrophenol to *p*-aminophenol using NaBH₄ in presence of catalyst AuNps obtained from AuCPH.

Rheological studies

The viscoelastic and mechanical properties of **CPH** have been investigated with dynamic oscillatory rheological measurements carried out on freshly prepared **CPH** metallohydrogels (1% w/v) (Figure 9). The Stress sweep experiment (25 °C, 1Hz) shows that the storage modulus (G') is ~ 1 order of magnitude higher than the loss modulus (G'') which proves the 'soft solid-like' nature of **CPH**.²³ The crossing observed above 1.4 Pa is moreover consistent with a mechanical damage of the gel structure or with a phase transition. Further, the elasticity of CPH were measured as a function of the strain amplitude ranging from -0.5% to 2.0% at 10 rad s⁻¹. The storage modulus (G') of about log 2.88 measured at small strain (f -0.5%) reveals the initial stability of the gel toward the shearing process. At constant frequency (1Hz), the gel was moreover found to be stable up to $\sim 1\%$ strain with negligible effect over elasticity, while further strain leads to a deformation process followed by a phase transition from gel to sol, as revealed by the steep decrease in the values of both moduli and by the reversal of the viscoelastic signal ($G'' > G'$).²⁴

Dynamic frequency sweep measurements carried out within the range 0.5- 1.5 rad s⁻¹ have revealed a linear and constant variation of G' and G'' with the applied frequency (ω), which indicates that the gel is made of a stable network.²⁵ The negative slope (-1) of plot the logarithmic plot of the complex viscosity (η^*) vs angular frequency (ω) also reveal a constant declination of the viscosity with increasing frequency.²⁶ The curve shown in figure 9F also suggests that the viscoelasticity of the sample remains unchanged between 25-60 °C and that a deformation starts to appear above 60 °C and reaches a maximum at 90 °C. The slow and long range deformation observed between 60 and 90 °C, might be the reason behind the reversible gel-sol transition observed with **CPH** (Figure S3 in supporting information). The critical temperature corresponding the gel/sol phase transition in CPH (T_{gel}) was estimated at 93 °C from the graph shown in figure 9F representing the loss tangent ($\tan \delta = G''/G'$) as a function of temperature.²⁷ The latter value and the thermal stability of the gel over a large temperature range was further confirmed with a plot of the complex viscosity versus temperature (Figure 9D).

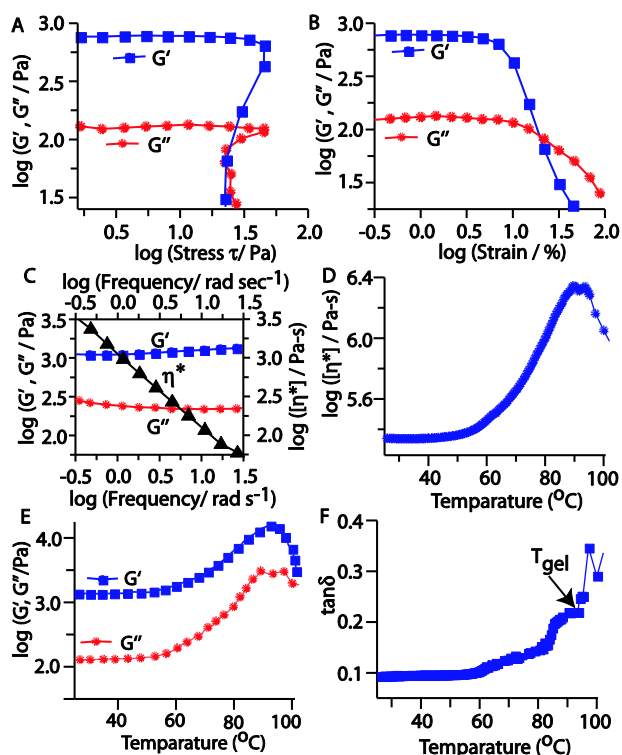


Figure 9. Rheology of CPH (A) Dynamic oscillation stress sweep of G' (Loss modulus) and G'' (Storage modulus) vs applied stress at frequency of 10 rad s^{-1} and temperature at $25 \text{ }^\circ\text{C}$, (B) Dynamic strain sweep experiment at 10 rad s^{-1} and temperature $25 \text{ }^\circ\text{C}$, (C) Primary axis: dynamic frequency sweep measurements of G' and G'' , at strain of 0.5% . Secondary axis: complex viscosity measurements, (D) Dynamic temperature ramp of complex viscosity measurement at $5 \text{ }^\circ\text{C min}^{-1}$, (E) Plot of G'' and G' on dynamic temperature ramp and (F) Dynamic temperature ramp of the loss tangent ($\tan \delta = G''/G'$) plot at $5 \text{ }^\circ\text{C min}^{-1}$.

Conductance studies

The conductance properties of freshly prepared **CPH** samples have been investigated by impedance measurements. The primary objective was to gain insights into the conductivity of the samples but also to follow the ageing phenomena, and to determine the influence of temperature and of the alkali ions on the electrical properties of the gels. The conductivity responses recorded over time with different LiOH, NaOH or KOH-based gel samples were found to follow the same trend, with a relatively fast decrease of the conductance in the first stage of the measurement (0-3h), leading to a loss of about 2-3% of the initial value, followed by an apparent stabilization on a longer time scale ($t > 4\text{h}$). Carrying out these time-dependent

measurements on a larger time scale still revealed a further drift of the conductivity values losing another 1-3 % over one week. To summarize, the conductivity of **CPH** as initiator have been found to be quite stable over time (t_0 : $507.6 \text{ mS}\cdot\text{m}^{-1} \rightarrow t_0 + 7 \text{ days}$: $489.9 \text{ mS}\cdot\text{m}^{-1}$). The reproducibility of the impedance responses has been checked with different samples synthesized following the same experimental procedure. The latter could be significantly improved upon developing a systematic synthetic procedure involving use of a programmable syringe pump enabling an accurate control over the addition rate of the Zn^{2+} solution. Most importantly, we found the electrical properties of the gels to be strongly dependent on the alkali metal ions used as initiators.^{9,10} This effect is clearly brought to light in figure 10 with data recorded for samples prepared with the same procedure involving either LiOH, NaOH, KOH or CsOH as key reactants. One of the conclusions drawn from these data is that the significant drop in the conductivity values observed along the series $\text{Cs}^+ > \text{K}^+ > \text{Na}^+ > \text{Li}^+$ is rather driven by the bulk properties of the gels than by the conductivity of their components. Based on simple visual observations, it was indeed established that the most rigid gels could systematically be obtained with LiOH while CsOH only led to hardly viscous solutions. The values plotted in figure 10 thus reveal the gelating ability of the different alkali ions used as initiators and not their intrinsic ionic conductivity (related to their mobility and decreasing in the following order $\text{Li}^+ > \text{Na}^+ > \text{K}^+ > \text{Cs}^+$). The most rigid gels obtained with Li^+ are thus less conductive on account of the restricted mobility of the charge carriers, while the most liquid samples obtained with Cs^+ give rise to much higher conductivity values. The conductivity of the Li^+ , Na^+ and K^+ based gels has been further investigated at different temperatures, between 293 and 343 K. As expected, the conductivity was found to increase with temperature in a similar manner for all the investigated samples. The linear evolution of the $\log \kappa = f(1/T)$ curves between 298K ($1000/T = 3.3$) and 323 K ($1000/T = 3.1$) (Figure 11) also support the conclusion that the gels samples are fully stable in this temperature range. The noticeable change in the slope of the $\log \kappa = f(1/T)$ curves observed beyond 343 K is then compatible with a significant modification of the gel sample induced upon heating. This conclusion is consistent with the rheology data discussed in the previous section, revealing that an increase in temperature leads to a hardening of the gel.

Similar impedance measurements have been carried out on **CPH** samples doped with Au nanoparticles (AuNPs) (Experimental section, Figure S16). The amount added (V_{AuNP}) was found to have a great influence on the properties and firmness of the resulting samples, going from well behaved gels (obtained for small V_{AuNP} values) to viscous or fully liquid solutions (obtained for large V_{AuNP} values).

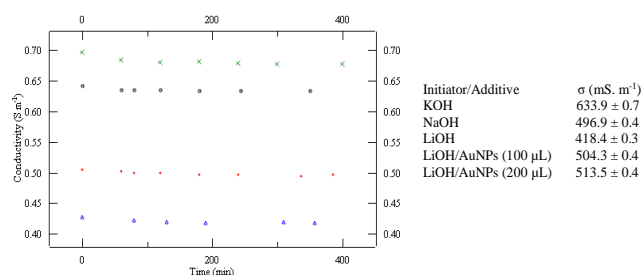
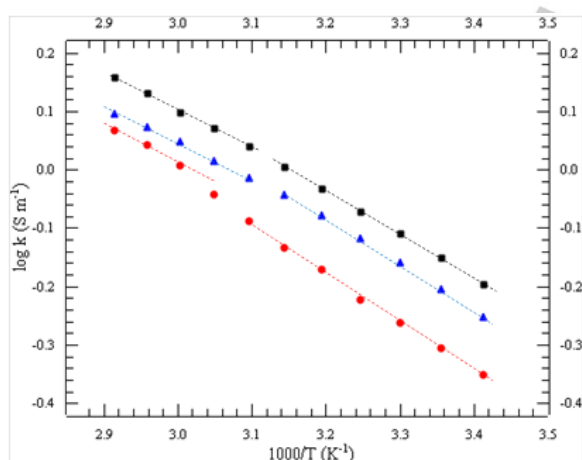


Figure 10. (Left) Cation dependence of the conductivity measured over time (0–400 min) on gel (Li^+ , Na^+ , K^+) or liquid (Cs^+) samples at 295K (green cross: CsOH, black square: KOH, red circle: NaOH, blue triangle: LiOH). (Right) Conductivity values (mS m^{-1}) measured at 295K and $t = 240$ min on four different gels produced from KOH, NaOH, LiOH, and LiOH + a given volume (V_{AuNP}) of a freshly prepared HAuCl_4 solution (HAuCl_4 , 10^{-1} mol L^{-1} in methanol/diethylether).

Figure 11. Temperature dependence (298–343 K) of the ionic conductivity measured on different gels samples (blue triangle: LiOH, red circle: NaOH, black square: KOH).

The amount added (V_{AuNP}) was found to have a great influence on the properties and firmness of the resulting samples, going from well behaved gels (obtained for small V_{AuNP} values) to viscous or fully liquid solutions (obtained for



large V_{AuNP} values) as demonstrated in figure S16. Suitable gel samples could be obtained repeatedly in these conditions for loadings (V_{Au}) falling in the range 100–200 μL . Suitable gel samples could be obtained repeatedly in these conditions for loadings (V_{Au}) falling in the range 100–200 μL . Impedance measurements carried out on these samples revealed that the addition of V_{AuNP} leads to a significant increase of the conductivity, *i.e.* from ~ 418 ms.m^{-1} measured in the absence of AuNPs to ~ 513 ms.m^{-1} measured on the gel sample prepared after addition of 200 μL of the HAuCl_4 solution. Here again, the improvement in conductivity could be attributed to changes in the steadiness of the gels rather than to the conductivity of the AuNPs.

Conclusions

In conclusion, we have synthesized a multi-stimuli responsive fluorescent metallohydrogel involving a coordination polymer as a key building element. The mechanism of gelation has been investigated using NMR, fluorescence, impedance, TEM and rheological measurements. The selective combination of $1/\text{Li}^+/\text{Zn}^{2+}$ was not only found to result in the fluorescence of the metallohydrogel, it also proved responsible for the formation of conducting nanometric fiber-shaped assemblies. These nanofibers have been used as growth platforms to achieve the fabrication of uniform sized AuNps (*ca.* 3–4 nm) in the absence of any external reducing agent. The AuNP-doped nanofibers have proved useful as catalytic material in the reduction of *p*-nitrophenol with NaBH_4 . The conductance properties of these metallohydrogels have also been explored and shown to be strongly dependent on the size of the alkali ions and on the temperature. We believe that this concept of metallohydrogel will open up new perspectives for the development and applications of soft materials in electronics and in catalysis.

Experimental Section

Materials and Physical Methods:

Reagents and solvents used in experiment were purchased from Sigma-Aldrich Chemicals Pvt. Ltd., Spectrochem Pvt. Ltd., and S. D. Chem-Limited. The solvents were distilled before using in synthesis by following standard sigma methods. Terephthaldehyde and D_2O were purchased from Sigma-Aldrich. L-Tyrosine and L-Phenylalanine were purchased from S. D. Chem-Limited and Spectrochem Pvt. Ltd., respectively.

FTIR and UV-Vis study of ligands were done on PerkinElmer-spectrum 100 FTIR and Thermo scientific evolution 200 spectrophotometer, respectively. Photoluminescence spectra were acquired on a Perkin Elmer LS 55 spectrophotometer. $^1\text{H-NMR}$ spectra were obtained on a Bruker AVANCE III HD 500 spectrometer. Electrospray ionization mass (ESI-MS) spectra were recorded on a Waters (Micromass MS Technologies) QToF Premier. Thermal Gravimetric analysis data was acquired on a NETZSCH TG209 F1 Libra TGA209FID-0105-l at a heating rate of 5 $^\circ\text{C min}^{-1}$ under a nitrogen atmosphere. TEM images were captured using a JEOL JEM 2100. Powder XRD data was collected on Rigaku SmartLab between angle $2\theta = 5$ – 80° . Rheology of metallohydrogel was performed on Anton Paar Quality Control Rheometer RheolabQC. Impedance measurements have been carried out with a Biologic® ESP 300 potentiostat equipped with a built-in computer-controlled Frequency Response Analyser (FRA) operating over a frequency range of 10 μHz up to 7 MHz.

Impedance measurements have been carried out with a Biologic® ESP 300 potentiostat equipped with a built-in computer-controlled Frequency Response Analyser (FRA) operating over a frequency range of 10 μHz up to 7 MHz. Home-made one-compartment, two-electrode cells allowing to position two identical cofacially oriented stainless steel or platinum electrodes at a fixed distance has been used

to estimate the conductivity of each sample. Variable temperature measurement of the conductivity have been carried out in a home-made jacketed glass cell incorporating two platinum electrodes ($\varnothing = 1\text{ cm}$). The temperature in the cell was controlled with a Lauda-Brinkman RE 104 thermostat. Electrical impedance measurements have been performed in a potentiostatic regime at E_{oc} between 1 Hz and 2.5 MHz using a maximum voltage of 0.01 V. Fitting the experimental Nyquist impedance diagrams ($-\text{Im}(Z)$ vs. $\text{Re}(Z)$) was achieved with Z-fit using equivalent electrical circuits involving the actual resistance of the sample R_1 , a capacitance C_1 and a constant-phase element Q_1 . Such fitting allowed to estimate the resistance of each samples corresponding to the intersection of the curve with the real part of the impedance. The conductivity was calculated from the electrolyte resistance (R_1) using the equation:

$$\sigma = l / R_1 \kappa$$

Where κ is the conductivity in $\text{S}\cdot\text{m}^{-1}$, R is the ohmic resistance of the electrolyte, l is the distance between the two electrodes (m) and S is the area of the electrodes (m^2). The cell constant, (l/S) was determined at 25°C by calibration with standard 0.001 D, 0.01 D and 0.1 D KCl solutions having known conductivity values, ($1408 \mu\text{S}\cdot\text{m}^{-1}$, $1285 \text{mS}\cdot\text{m}^{-1}$ and $11.13 \text{S}\cdot\text{m}^{-1}$).

Synthesis of $\text{H}_4\text{T}^{\text{L-tyr}}(1)$: It was synthesized by following the standard literature with some modification. L -tyrosine (0.200 g, 1.1 mmol) and $\text{LiOH}\cdot\text{H}_2\text{O}$ (0.069 g, 1.64 mmol) were dissolved in dry methanol (15 mL) and stirred for 15 min at room temperature. Methanolic solution of terephthaldehyde (0.185 g, 1.37 mmol) was added the above solution and stirred for an additional 5 hours. Resulting mixture was reduced with sodium borohydride (0.168 g, 4.412 mmol). Upon neutralisation with dilute HCl, it afforded a white solid, thoroughly washed with water, diethylether and dried under vacuum. Yield 0.440 g (85%). Anal. Calc. for $\text{C}_{26}\text{H}_{28}\text{N}_2\text{O}_6$: C, 67.21; H, 6.07; N, 6.03. Found C, 68.02; H, 6.83; N, 5.79. Due to poor solubility of the neutral form, $^1\text{H-NMR}$ and UV-vis measurements were performed by dissolving the solid in D_2O in presence of 3 equiv. of $\text{LiOH}\cdot\text{H}_2\text{O}$. $^1\text{H NMR}$ (500 MHz, D_2O , ppm): δ 7.27 (s, 4H, Ar), 6.95 (d, 4H, Ph), 6.54 (d, 4H, Ph), 3.72 (d, 2H, $-\text{CH}_2\text{Ph}$), 3.54 (d, 2H, $-\text{CH}_2\text{Ph}$), 3.28 (t, 2H, $-\text{CHNH}$), 2.75 (m, 4H, $-\text{CH}_2\text{NH}$). IR (KBr, cm^{-1}) $\nu_{\text{as}}(\text{COO})$ 1615(s). UV-vis [water, λ_{max} , nm (ϵ , $\text{M}^{-1} \text{cm}^{-1}$): 275 (2800), 222sh.

Synthesis of $\text{H}_4\text{T}^{\text{L-phe}}(2)$. It was synthesized following the above procedure for $\text{H}_4\text{T}^{\text{L-tyr}}(1)$ using L -phenylalanine instead of L -tyrosine. Yield 0.480 g (92%). Anal. calcd for $\text{C}_{26}\text{H}_{28}\text{N}_2\text{O}_4$: C, 72.20; H, 6.53; N, 6.48. Found C, 72.88; H, 7.02; N, 6.37. Due to poor solubility of the neutral form, $^1\text{H NMR}$ and UV-vis measurements were performed by dissolving the solid in D_2O in presence of 2 eqv. of $\text{LiOH}\cdot\text{H}_2\text{O}$. $^1\text{H NMR}$ (D_2O , ppm): δ 7.35-7.21 (m, 14H, Ar & Ph), 3.72 (d, 2H, $-\text{CH}_2\text{Ph}$), 3.54 (d, 2H, $-\text{CH}_2\text{Ph}$), 3.34 (t, 2H, $-\text{CHNH}$), 2.89 (m, 4H, $-\text{CH}_2\text{NH}$). IR (KBr, cm^{-1}) $\nu_{\text{as}}(\text{COO})$ 1570(s). UV-vis. [water, λ_{max} , nm (ϵ , $\text{M}^{-1} \text{cm}^{-1}$): 260 (1200).

Synthesis of metallohydrogel (CPH). $\text{H}_4\text{T}^{\text{L-tyr}}(1)$ (0.010 g, 0.021 mmol) was suspended in water (300 μL), which made clear through addition of aqueous $\text{LiOH}\cdot\text{H}_2\text{O}$ (0.0027 g, 0.065 mmol, 200 μL). Further, very cautiously, add drop wise aqueous $\text{Zn}(\text{NO}_3)_2$ (0.0064 g, 0.021 mmol, 500 μL) to the above transparent solution which form transparent metallohydrogel (1% w/v) instantly, after complete addition. Furthermore, gelation was confirmed by the 'inverted vial method'. The complex was isolated by drying gel followed by washing with water and diethyl ether to remove in situ formed impurities. The pure isolated complex was used for further analytical characterization. Anal. Calc. for $[\text{Zn}(\text{C}_{26}\text{H}_{28}\text{N}_2\text{O}_6)(\text{H}_2\text{O})_3]$: C, 53.78; H, 5.55; N, 4.82. Found C, 53.67; H,

5.43; N, 4.91. ESI-MS (diluted gel) m/z [$\text{H}_3\text{T}^{\text{L-tyr}}\text{Zn}$] $^+$, 527.1 (calc. 527.1); [$\text{H}_3\text{T}^{\text{L-tyr}}+\text{Zn}_2+\text{NO}_3+\text{H}_2\text{O}$] $^+$, 675.2 (calc. 675.2). IR (KBr, cm^{-1}) $\nu_{\text{as}}(\text{COO})$ 1631(s). Weight loss as per TGA: 10.46 % (calc. for $3\text{H}_2\text{O}$: 10.21 %). UV-vis [water, λ_{max} , nm (ϵ , $\text{M}^{-1} \text{cm}^{-1}$): 275 (2800), 222br.

Synthesis of Gold nanoparticle embedded metallohydrogel (AuCPH). Synthesis of AuCPH involved, as a last step prior to gelification of CPH, the slow addition of a given volume (V_{AuNP}) of a freshly prepared HAuCl_4 solution (HAuCl_4 , 10^{-1}molL^{-1} in methanol/diethylether, 100 μL -400 μL) to a mixture of ligand, LiOH and Zn^{2+} salt. An instant and drastic change in colour of CPH from white to red was obtained without disturbance in appearance of CPH. The AuCPH was further subjected to characterization with suitable instrumental techniques like IR (KBr, cm^{-1}): $\nu_{\text{as}}(\text{COO})$ 1615(s). UV-vis [water, λ_{max} , nm (ϵ , $\text{M}^{-1} \text{cm}^{-1}$): 275 (2400), 560 br. TEM: diameter of nanoparticle $\sim 3 \text{ nm}$.

TEM sample preparation

Samples for TEM analysis was prepared by diluting 1 mL of gel in a 15 mL water. 1 to 3 drops of this solution were placed on a carbon-coated copper grid (400 mesh) and dried in dust free vacuum for 2 days. After complete drying, the specimens were examined with a JEOL JEM-2100 transmission electron microscope operating at 200 kV using an accelerating voltage of 100 kV and a 16 mm working distance.

Acknowledgements

M. Dubey acknowledges the Department of Science and Technology, New Delhi, India, for research grant under DST-INSPIRE Faculty award. MKD acknowledges IIT (BHU) and MHRD for fellowship. We acknowledge SIC IIT Indore, CIF IIT (BHU) Varanasi and AMU Aligarh for extending the instrumental facilities.

Keywords: metallohydrogel • fluorescence • nanofabrication • nanoparticle • catalysis • conductance

- [1] a) Z. Y. Li, Y. Zhang, C. W. Zhang, L. J. Chen, C. Wang, H. Tan, Y. Yu, X. Li and H. B. Yang, *J. Am. Chem. Soc.*, **2014**, *136*, 8577; b) J. A. Foster, R. M. Parker, A. M. Belenguer, N. Kishi, S. Sutton, C. Abell and J. R. Nitschke, *J. Am. Chem. Soc.*, **2015**, *137*, 9722; c) S. Datta, M. L. Saha and P. J. Stang, *Acc. Chem. Res.*, **2018**, *51*, 9, 2047; d) X. Yan, T. R. Cook, J. B. Pollock, P. Wei, Y. Zhang, Y. Yu, F. Huang and P. J. Stang, *J. Am. Chem. Soc.*, **2014**, *136*, 4460; e) W. J. Rieter, K. M. Pott, K. M. L. Taylor and W. Lin, *J. Am. Chem. Soc.*, **2008**, *130*, 11584; f) B. O. Okesol and D. K. Smith, *Chem. Soc. Rev.*, **2016**, *45*, 4226; g) T. Tu, W. Fang, X. Bao, X. Li and K. H. Dötz, *Angew. Chem. Int. Ed.*, **2011**, *50*, 6601; h) Q. Lin, T. T. Lu, X. Zhu, B. Sun, Q. P. Yang, T. B. Wei and Y. M. Zhang, *Chem. Commun.*, **2015**, *51*, 1635.
- [2] a) J. W. Steed, *Chem. Soc. Rev.*, **2010**, *39*, 3686; b) A. Y. Y. Tam and V. W. W. Yam, *Chem. Soc. Rev.*, **2013**, *42*, 1540; c) M. M. Piepenbrock, G. O. Lloyd, N. Clarke and J. W. Steed, *Chem. Rev.*, **2010**, *110*, 1960; d) V. K. Praveen, C. Ranjith and N. Armaroli, *Angew. Chem., Int. Ed.*, **2014**, *53*, 365; e) V. K. Pandey, M. K. Dixit, S. Manneville, C. Bucher and M. Dubey, *J. Mater. Chem. A*, **2017**, *5*, 6211; f) M. O. M. Piepenbrock, N. Clarke and J. W. Steed, *Soft Matter*, **2011**, *7*, 2412; g) J. H. Lee, S. Kang, J. Y. Lee and J. H. Jung, *Soft Matter*, **2012**, *8*, 6557; h) M. Paul, K. Sarkar and P. Dastidar, *Chem. Eur. J.*, **2015**, *21*, 255; i) L. Yang, L. Luo, S. Zhang, X. Su, J. Lan, C. T. Chen and J. You, *Chem. Commun.*, **2010**, *46*, 3938; j) C. K. Karan and M. Bhattacharjee, *ACS Appl. Mater. Interfaces*, **2016**, *8*, 5526; k) W. J. Gee and S. R. Batten, *Chem. Commun.*, **2012**, *48*, 4830; l) A. Biswas, M. Dubey, S. Mukhopadhyay, A. Kumar and D. S. Pandey, *Soft Matter*, **2016**, *12*, 2997.

- [3] a) C. Largeot, C. Portet, J. Chmiola, P. Taberna, Y. Gogotsi and P. Simon, *J. Am. Chem. Soc.*, **2008**, *130*, 2730; b) S. Kandalkar, D. Dhawale, C. Kim and C. Lokhande, *Synth. Met.*, **2010**, *160*, 1299; c) G. Wang, L. Zhang and J. Zhang, *Chem. Soc. Rev.*, **2012**, *41*, 797; d) T. Schoetz, M. Kurniawan, M. Stich, R. Peipmann, I. Efimov, A. Ispas, A. Bund, C. P. D. Leon and M. Ueda, *J. Mater. Chem. A*, **2018**, *6*, 17787; e) K. Takei, T. Takahashi, J. C. Ho, H. Ko, A. G. Gillies, P. W. Leu, R. S. Fearing, A. Javey, *Nat. Mater.*, **2010**, *9*, 821.
- [4] a) S. Saha, E. M. Schçn, C. Cativiela, D. D. Diaz and R. Banerjee, *Chem. Eur. J.*, **2013**, *19*, 9562; b) H. B. Aiyappa, S. Saha, P. Wadge, R. Banerjee and S. Kurungot, *Chem. Sci.*, **2015**, *6*, 603.
- [5] a) J. M. Tarascon and M. Armand, *Nature*, **2001**, *414*, 359; b) Y. S. Kim, Y. G. Cho, D. Odkhuu, N. Park and H. K. Song, *Sci. Rep.*, **2013**, *3*, 1917; c) X. Zhao, F. Chen, Y. Li, H. Lu, N. Zhang and M. Ma, *Nat. Commun.*, **2018**, *9*, 3579; d) S. K. M. Nalluri, N. Shivarova, A. L. Kanibolotsky, M. Zelzer, S. Gupta, P. W. J. M. Frederix, P. J. Skabara, H. Gleskova and R. V. Ulijn, *Langmuir*, **2014**, *30*, 12429; e) J. P. Luis, V. Laukhin, A. P. D. Pino, J. V. Gancedo, C. Rovira, E. Laukhina and D. B. Amabilino, *Angew. Chem. Int. Ed.*, **2007**, *46*, 238; f) A. Rahimi, A. H. Arbeitman and J. M. García, *Macromol. Mater. Eng.*, **2019**, *304*, 1800583; g) S. Dhibar, A. Dey, S. Majumdar, D. Ghosh, A. Mandal, P. P. Ray and B. Dey, *Dalton Trans.*, **2018**, *47*, 17412.
- [6] a) T. Sekitani, T. Yokota, K. Kuribara, M. Kaltenbrunner, T. Fukushima, Y. Inoue, M. Sekino, T. Isoyama, Y. Abe, H. Onodera and T. Someya, *Nat. Commun.*, **2016**, *7*, 11425; b) Xu Peng, Huili Liu, Qin Yin, Junchi Wu, Pengzuo Chen, Guangzhao Zhang, Guangming Liu, Changzheng Wu and Yi Xie, *Nat. Commun.*, **2016**, *7*, 11782; c) Y. Gu, S. Zhang, L. Martinetti, K. H. Lee, L. D. McIntosh, C. D. Frisbie and T. P. Lodge, *J. Am. Chem. Soc.*, **2013**, *135*, 9652.
- [7] a) B. Xing, M. F. Choi and B. Xu, *Chem. Eur. J.*, **2002**, *8*, 5028; b) L. Yang, L. Luo, S. Zhang, X. Su, J. Lan, C. T. Chen and J. You, *Chem. Commun.*, **2010**, *46*, 3938; c) Y. M. A. Yamada, Y. Maeda and Y. Uozumi, *Org. Lett.*, **2006**, *8*, 4259.
- [8] a) Md. H. Rashid and T. K. Mandal, *Adv. Funct. Mater.*, **2008**, *18*, 2261; b) R. Ciganda, N. Li, C. Deraedt, S. Gatard, P. Zhao, L. Salmon, R. Hernandez, J. Ruiza and D. Astruc, *Chem. Commun.*, **2014**, *50*, 10126; c) J. Lee, J. C. Park and H. Song, *Adv. Mater.*, **2008**, *20*, 1523; d) Y. Choi, H. S. Bae, E. Seo, S. Jang, K. H. Park and B. S. Kim, *J. Mater. Chem.*, **2011**, *21*, 15431; e) R. Fenger, E. Fertitta, H. Kirmse, A. F. Thunemann and K. Rademann, *Phys. Chem. Chem. Phys.*, **2012**, *14*, 9343.
- [9] a) M. Dubey, A. Kumar, R. K. Gupta and D. S. Pandey, *Chem. Commun.*, **2014**, *50*, 8144; b) M. K. Dixit, V. K. Pandey and M. Dubey, *Soft Matter*, **2016**, *12*, 3622; c) M. K. Dixit and M. Dubey, *Phys. Chem. Chem. Phys.*, **2018**, *20*, 23762; d) M. Dubey and M. Ray, *CrystEngComm*, **2013**, *15*, 9648.
- [10] a) L. Brigo, M. Cittadini, L. Artiglia, G. A. Rizzi, G. Granozzi, M. Guglielmi, A. Martucci and G. Brusatin, *J. Mater. Chem. C*, **2013**, *1*, 4252; b) D. Jaque, L. M. Maestro, B. d. Rosal, P. H. Gonzalez, A. Benayas, J. L. Plaza, E. M. Rodriguez and J. G. Sole, *Nanoscale*, **2014**, *6*, 9494; c) L. Chen, C. P. Deming, Y. Peng, P. Hu, J. Stofan and S. Chen, *Nanoscale*, **2016**, *8*, 14565.
- [11] J. D. S. Newman and G. J. Blanchard, *Langmuir*, **2006**, *22*, 5882.
- [12] a) X. Wang, T. He, L. Yang, H. Wu, R. Zhang, Z. Zhang, R. Shen, J. Xiang, Y. Zhang and C. Wei, *Nanoscale*, **2016**, *8*, 6479; b) X. Wang, T. He, L. Yang, H. Wu, J. Yin, R. Shen, J. Xiang, Yi Zhang and C. Wei, *Dalton Trans.*, **2016**, *45*, 18438.
- [13] E. Beltran, M. Garzoni, B. Feringan, A. Vancheri, J. Barbera, J. L. Serrano, G. M. Pavan, R. Gimenez and T. Sierra, *Chem. Commun.*, **2015**, *51*, 1811.
- [14] a) M. H. Chan, M. Ng, S. Y. Leung, W. H. Lam and V. W. W. Yam, *J. Am. Chem. Soc.*, **2017**, *139*, 8639; b) W. Fang, Z. Sun, T. Tu, *J. Phys. Chem. C*, **2013**, *117*, 25185; c) X.S. Xiao, W. Lu, C. M. Che, *Chem. Sci.*, **2014**, *5*, 2482.
- [15] a) J. H. Lee, H. Lee, S. Seo, J. Jaworski, M. L. Seo, S. Kang, J. Y. Lee, J. H. Jung, *New J. Chem.*, **2011**, *35*, 1054; b) S. K. Batabyal, W. L. Leong, J. J. Vittal, *Langmuir*, **2010**, *26*, 7464.
- [16] X. Ma, R. Sun, J. Cheng, J. Liu, F. Gou, H. Xiang and X. Zhou, *J. Chem. Educ.*, **2016**, *93*, 345.
- [17] M. Dubey, A. Kumar and D. S. Pandey, *Chem. Commun.*, **2014**, *50*, 1675.
- [18] a) Y. Sun, S. Li, Z. Zhou, M. L. Saha, S. Datta, M. Zhang, X. Yan, D. Tian, H. Wang, L. Wang, X. Li, M. Liu, H. Li and P. J. Stang, *J. Am. Chem. Soc.*, **2018**, *140*, 3257.
- [19] H. Basit, A. Pal, S. Sen and S. Bhattacharya, *Chem. Eur. J.*, **2008**, *14*, 6534.
- [20] P. Thordarson, *Chem. Soc. Rev.*, **2011**, *40*, 1305.
- [21] a) J. Liu, G. Qin, P. Raveendran and Y. Ikushima, *Chem. Eur. J.* **2006**, *12*, 2131; b) R. K. Gupta, M. Dubey, P. Z. Li, Q. Xu and D. S. Pandey, *Inorg. Chem.* **2015**, *54*, 2500.
- [22] a) N. Sahiner, H. Ozay, O. Ozay and Nahit Aktas, *Applied Catalysis A*, **2010**, *385*, 201; b) H. E. Prysztajn and R. M. Negri, *J. Chem. Educ.*, **2001**, *78*, 645.
- [23] a) S. Basak, J. Nanda and A. Banerjee, *J. Mater. Chem.*, **2012**, *22*, 11658.
- [24] C. Rizzo, F. D'Anna, R. Noto, M. Zhang and R. G. Weiss, *Chem. Eur. J.*, **2016**, *22*, 11269.
- [25] F. M. Menger, and K. L. Caran, *J. Am. Chem. Soc.* **2000**, *122*, 11679.
- [26] a) S. Srinivasan, S. S. Babu, V. K. Praveen, A. Ajayaghosh, *Angew. Chem., Int. Ed.* **2008**, *47*, 5746; b) A. Jaishankar and G. H. McKinley, *Proc. R. Soc. A*, **2012**, 20120284. 4.
- [27] M. Zhang, L. Meng, X. Cao, M. Jiang and T. Yi, *Soft Matter*, **2012**, *8*, 449.

FULL PAPER

Entry for the Table of Contents (Please choose one layout)

Layout 1:

FULL PAPER

Text for Table of Contents

((Insert TOC Graphic here: max.
width: 5.5 cm; max. height: 5.0 cm))

*Author(s), Corresponding Author(s)**

Page No. – Page No.

Title

Layout 2:

FULL PAPER

((Insert TOC Graphic here; max. width: 11.5 cm; max. height: 2.5 cm))

*Author(s), Corresponding Author(s)**

Page No. – Page No.

Title

Text for Table of Contents
